

June 2003

Analysis and Simulation of Anode Heating Due to Electron Field Emission

Timothy Fisher

Birck Nanotechnology Center and School of Mechanical Engineering, Purdue University, tsfisher@purdue.edu

D. G. Walker

Vanderbilt University

Robert A. Weller

Vanderbilt University

Follow this and additional works at: <http://docs.lib.purdue.edu/nanopub>

Fisher, Timothy; Walker, D. G.; and Weller, Robert A., "Analysis and Simulation of Anode Heating Due to Electron Field Emission" (2003). *Birck and NCN Publications*. Paper 54.
<http://docs.lib.purdue.edu/nanopub/54>

This document has been made available through Purdue e-Pubs, a service of the Purdue University Libraries. Please contact epubs@purdue.edu for additional information.

Analysis and Simulation of Anode Heating Due to Electron Field Emission

Timothy S. Fisher, D. G. Walker, and Robert A. Weller

Abstract—This paper considers the effect of anode heating from energetic electrons produced by field emission. Large electric fields accelerate emitted electrons as they traverse the vacuum gap toward the anode. Electron energy is transferred to the anode by collisions with the lattice. The nonequilibrium transfer of electron kinetic energy to anode thermal energy is examined quantitatively. Results demonstrate that the energy distribution of impinging electrons affects the transmission and dissipation of thermal energy. A Monte Carlo technique is used to resolve the thermalization of electrons and accounts for electron beam strength and spatial distribution. The results indicate that local heat fluxes of the order 10 kW/cm^2 occur at the anode surface and that heating is a strong function of field strength because of the exponential relationship between applied voltage and current. Under practical conditions, temperature increases of $10 \text{ }^\circ\text{C}$ are predicted from a single point emission source.

Index Terms—Anode heating, electron field emission, Monte Carlo.

NOMENCLATURE

A	Emission area (nm^2).
g	Generation rate (W/nm^2).
h	Planck's constant.
j	Current density (A/nm^2).
k	Thermal conductivity ($\text{W}/\text{nm}^2\text{K}$).
L	Vacuum gap dimension (nm).
m	Electron rest mass ($9.1 \times 10^{-31} \text{ kg}$).
N	Number of electrons.
p	Electron momentum.
q	Electron charge ($1.6 \times 10^{-19} \text{ C}$).
q''	Heat flux (W/m^2).
V	Potential (V).
x	Longitudinal coordinate (nm).

Greek Letters

α	Emission angle.
β	Local field enhancement factor.
ϵ	Electron energy (eV).
κ	Thermal diffusivity (nm^2/sec).

μ	Chemical potential (eV).
ϕ	Work function (eV).
ρ	Radial coordinate (nm).
θ	Polar angle.
ψ	Azimuthal angle.
Ω	Solid angle.

I. INTRODUCTION

FIELD emission devices have been used and contemplated for a wide range of electronic device applications, including flat-panel displays, scanning probe tips, and power diodes and transistors [1], [2]. Cathode materials such as carbon nanotubes and polycrystalline diamond exhibit high rates of electron emission at relatively low applied electric fields. This emission, however, is typically localized to specific sites on the cathode where high levels of local electric field enhancement are present. This localization of emission can create extremely high current density in the cathode. The flow of emitted electrons then accelerates in the vacuum gap between the cathode and anode due to the electric field. Consequently, a highly energetic and localized stream of electrons bombards the anode and can cause substantial heating that may lead to failure. The present work describes in detail the spatial and energetic distribution of field-emitted electrons and presents simulations of localized anode heating due to ballistic electron bombardment. The results indicate high levels of heat dissipation and temperature rise under practical device conditions.

Field emission of electrons from a surface involves quantum tunneling through a potential barrier into vacuum. The potential field is created by an anode at a lower electron potential, as shown in Fig. 1. Fowler and Nordheim [3] described the physics of field emission from a planar metallic surface. Later, researchers found that elongated emitter structures can substantially enhance emission by increasing the local electric field near the tip of the emitter [4]. In recent years, field emission from a variety of materials, including metals and semiconductors, has been studied.

Field emission devices show promise in a number of technically important applications. Jensen [5] provided a recent review of applications in electronics. Due to the high electron mobility in vacuum, vacuum integrated circuits could provide significant increases in speed as compared to solid-state integrated circuits. Also, field emission arrays are capable of providing power amplification at very high frequencies (up to tens of GHz) and may also be useful as part of plasma-thruster systems for space propulsion. Field emitters also offer advantages in microwave power tube applications (e.g., travelling wave tubes) due to their

Manuscript received June 1, 2002; revised January 13, 2003. This work was supported in part by an NSF Career Award (CTS-9983961), DARPA/ARO (DAAD190110639) and a Vanderbilt University Discovery Grant. This work was recommended for publication by Associate Editor C. Amon upon evaluation of the reviewers' comments.

T. S. Fisher is with the School of Mechanical Engineering, Birck Nanotechnology Center, Purdue University, West Lafayette, IN 47907 USA (e-mail: tsfisher@purdue.edu).

D. G. Walker is with the Department of Mechanical Engineering, Vanderbilt University, Nashville, TN 37235 USA.

R. A. Weller is with the Department Electrical Engineering and Computer Science, Vanderbilt University, Nashville, TN 37235 USA.

Digital Object Identifier 10.1109/TCAPT.2003.815090

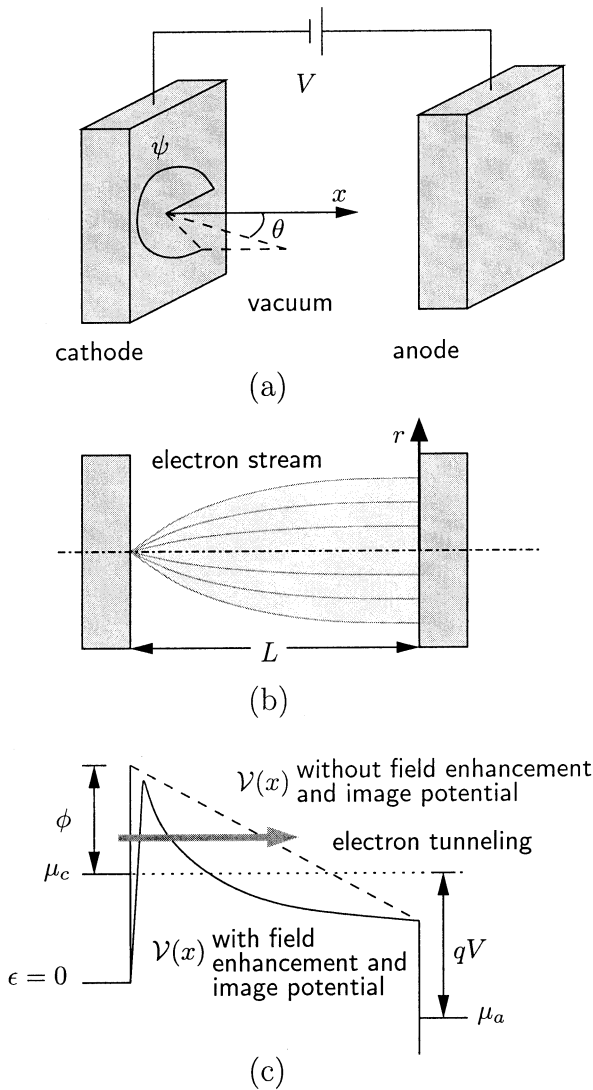


Fig. 1. Schematic representation of field emission between a cathode and anode separated by vacuum. (a) Sketch of planar cathode and anode showing spherical-polar coordinate system at the cathode surface. (b) Side-view schematic of the electron stream and radial coordinate at the anode surface. (c) Electron potential energy distribution from cathode to anode.

ability to transmit higher current densities and breakdown voltages than traditional technologies [6]. In addition, field emission arrays show much promise as practical electron sources for flat-panel displays [7], [8].

Carbon-based materials have been shown to be excellent field emitters. Polycrystalline diamond emitters exhibit high current density at low applied fields [9], and monolithic three-terminal devices based on molded diamond nanotip emitters have been shown to produce excellent transistor behavior [10]. Recent research on carbon nanotubes indicates that they can support local current densities as high as 10^9 A/cm² [11], [12], and experiments suggest that field emission current densities from emitter arrays could exceed 10^5 A/cm² [13]. Carbon nanotubes are also very efficient field emitters, with turn-on fields below 5 V/ μ m [14]. Interestingly, the cross-sectional current from single-walled carbon nanotubes reveals a ring-like current density, indicative of emission from the nanotube ends [13], [15]. This behavior produces extremely large local current

densities within the ring and is not observed for other field emitter materials.

One historical impediment to the application of field emission devices has been their poor reliability. Common failure modes include erosion of tip emitters [2] and anodes [16] due to excessive local current densities. These problems can be alleviated through the use of emitter materials, such as carbon nanotubes and polycrystalline diamond, that can tolerate high current densities and through an improved understanding of the energy dissipation processes in the anode.

The present work considers in detail the process of energy dissipation in the anode. The theoretical development, described in the Theory section, involves modeling of the spatial and energetic distribution of electrons from a localized emission site and the modification of the distribution through the accelerating field in the vacuum gap prior to deposition in the anode. Based on this distribution, the heat deposition process in the anode is modeled by a Monte Carlo electron scattering algorithm coupled with a heat diffusion solver. The resulting combined model is then used to simulate heat transfer under a variety of practical operating conditions.

II. THEORY AND ANALYSIS

A. Field Emission

Good and Müller [17] provided a comprehensive review of field emission theory from first principles. In the following paragraphs, we include elements of the theory that are necessary to describe the energetic and spatial distributions of field-emitted electrons from a point source. Following the above-cited work, we assume emission from a planar free-electron metal such that the emission distribution is spatially separable.

The number of electrons within a metal striking a surface represents the supply of electrons available for emission and can be calculated as [17]

$$N = \frac{2}{mh^3} \int_0^\infty \int_{-\infty}^\infty \int_{-\infty}^\infty p_x f(\epsilon) dp_x dp_y dp_z \quad (1)$$

where p_i represents electron momentum in the three Cartesian coordinates $i = x, y, z$, $f(\epsilon)$ is the Fermi-Dirac distribution function, m is the electron rest mass, and h is Planck's constant. The direction x represents the primary direction of emission into vacuum (see Fig. 1). Using the kinetic relation between energy and momentum, $\epsilon = p^2/2m$, and transforming from Cartesian to spherical-polar coordinates, the differential supply function N' becomes

$$N' = \frac{4m}{h^3} \epsilon f(\epsilon) \sin \theta \cos \theta d\epsilon d\theta d\psi \quad (2)$$

where θ is the spherical-polar angle [see Fig. 1(a)] relative to the surface-normal direction and ψ is the azimuthal angle. The foregoing expression represents the number of electrons striking the surface ($0 < \theta \leq \pi/2$, $0 < \psi \leq 2\pi$) per unit time per unit area within the energy range $(\epsilon, \epsilon + d\epsilon)$ and within the solid angle range $(\Omega, \Omega + d\Omega)$, where $d\Omega = \sin \theta d\theta d\psi$.

The transmission coefficient $D(\epsilon_x)$ defines the probability that an electron with an x-component of energy flux $\epsilon_x = \epsilon \cos^2 \theta$ will tunnel from the solid into vacuum. The transmission coefficient depends strongly on the width of the potential barrier encountered by the electron. In the present work, we employ the WKB approximation for the transmission coefficient [17]

$$D(\epsilon_x) = \exp \left\{ - \int_{x_1}^{x_2} \sqrt{\frac{8m}{\hbar^2} |\mathcal{V}(x) - \epsilon_x|} dx \right\} \quad (3)$$

where x_1 and x_2 are the zeroes of $\mathcal{V}(x) - \epsilon_x$ such that $x_2 - x_1$ represents the local width of the barrier. The potential $\mathcal{V}(x)$ is approximated near the location of emission at the cathode as [17]

$$\mathcal{V}(x) = -q\beta \frac{V}{L} x - \frac{q^2}{16\pi\epsilon_0 x} + \mu_c + \phi \quad (4)$$

where β is the local field enhancement factor, V is the applied bias, L is the gap width, μ_c is the cathode's chemical potential, ϕ is the cathode's work function, q is the magnitude of electron charge, and ϵ_0 is the permittivity of vacuum. The field enhancement factor β represents the factor by which the applied field V/L is multiplied to represent the local electric field near the emission point. This enhancement can be produced by nanometer-scale protrusions on the cathode.

The product of the transmission coefficient of (3) and the differential supply function of (2) provides the number of electrons emitted per second per unit area per unit energy per unit solid angle

$$F(\theta, \epsilon) = \frac{N' D(\epsilon_x)}{d\epsilon d\Omega} = \frac{4m}{\hbar^3} \epsilon f(\epsilon) D(\epsilon \cos^2 \theta) \cos \theta. \quad (5)$$

We note that $F(\theta, \epsilon)$ is similar in form and function to intensity in radiation heat transfer. This function can be integrated over energy and solid angle to provide the emitted current density

$$j = q \int_0^\infty \int_0^{\frac{\pi}{2}} \int_0^{2\pi} F(\theta, \epsilon) \sin \theta d\epsilon d\theta d\psi. \quad (6)$$

where ψ is the azimuthal angle of emission (see Fig. 1).

The transport of electrons from the cathode to the anode is treated classically. We assume that the cathode and anode are parallel planes positioned a distance L apart and biased by a voltage V (see Fig. 1), with the cathode chosen as the reference. The localized region of emission on the cathode is assumed to be a point source emitting electrons with an angular and energy distribution given by (5) for $F(\theta, \epsilon)$, where θ is the spherical-polar angle, with $\theta = 0$ corresponding to emission normal to the surface, and ϵ is the energy of emitted electrons. The emission is assumed to be azimuthally symmetric.

The essence of the transport problem in the vacuum gap is to relate the rate of electron impacting the anode per unit area per unit energy at distance ρ from the common axis—a quantity represented below by $G(\rho, E)$ —to the emission distribution $F(\theta, \epsilon)$. For the simple geometry assumed here, this transformation of an angular to a spatial distribution can be achieved analytically.

Assuming a unidirectional electric field, the relationship between the emitted electron energy ϵ and the energy E at anode impact is trivial: $\epsilon = E - V$. The relationship between ρ and the emission angle θ , or more conveniently between ρ and $\alpha = \cos \theta$, is central to determining the spatial distribution of electrons impacting the anode. For any given value of ϵ , the greatest impact distance ρ will occur when the emission is parallel to the surface ($\theta = \pi/2$). Consequently, at any given radius, a lower energy cutoff exists as given by

$$E_{min} = V \left(1 + \frac{\rho^2}{4L^2} \right). \quad (7)$$

For convenience, the variable τ is defined as

$$\tau = \sqrt{4E(E - V) - \frac{V^2 \rho^2}{L^2}}. \quad (8)$$

With this definition, the relationship between impact radius and emission angle becomes

$$\alpha = \cos \theta = \frac{\sqrt{4L^2(E - V) - \rho^2(\tau + 3V - 2E)}}{2\sqrt{(E - V)(L^2 + \rho^2)}}. \quad (9)$$

The Jacobian of the transformation follows from this relation as

$$J = \frac{3L^2 V^2 \rho^2 + V^2 \rho^4 + d^4(8E^2 - 8EV + 4E\tau - 2V\tau)}{8L^2(E - V)(L^2 + \rho^2)^2 \tau \alpha}. \quad (10)$$

The relation between G and F can thus be expressed as

$$G(\rho, E) = F \{ \arccos[\alpha(\rho, E)], E - V \} J, \quad (11)$$

$$E \geq V \left(1 + \frac{\rho^2}{4L^2} \right)$$

and $G(\rho, E) = 0$ otherwise. The function $G(\rho, E)$ represents the rate of electron impact on the anode per unit energy per unit anode area, $dA = 2\pi\rho d\rho$, per unit emission area at the cathode. In this work, we assume a cathode emission area $A_c = 100 \text{ nm}^2$ for all conditions. Thus, the local current density at the anode can be expressed as

$$j_a(\rho) = A_c \int_0^\infty qG(\rho, E) dE. \quad (12)$$

The total current I can then be computed by integrating (12) over the surface area.

The foregoing development ignores space-charge broadening of the beam. This effect becomes significant as total current increases. The exact inclusion of space-charge effects for the types of electron beams considered here is quite challenging due to the nonuniformity of the beam and its acceleration from the applied bias [18]. However, the magnitude of space-charge broadening can be estimated in a reasonably straightforward manner by assuming a linearly diverging beam of uniform current cross-section. The broadening can be characterized by the change in radial position $\Delta\rho$ of a point in the beam compared to the unperturbed radial location ρ [18]

$$\Delta\rho \sim 2\rho_0 \lambda \left(R \frac{\rho}{\rho_0} + A \frac{\gamma}{\gamma_0} \right)$$

where

$$\begin{aligned} A &= K + \frac{K}{1+K} - 2 \ln(1+K), \quad \gamma_0 = \arctan \frac{\rho_0}{L}, \\ R &= \ln(1+K) + \frac{K}{1+K}, \quad \gamma = \arctan \frac{\rho}{L}, \\ \lambda &= \frac{m^{\frac{1}{2}} I}{2^{\frac{1}{2}} \pi \epsilon_0 q^{\frac{1}{2}} \gamma_0^2 V^{\frac{3}{2}}}, \quad K = \frac{-\gamma_0 L}{r_0}. \end{aligned} \quad (13)$$

In the foregoing equations, ρ_0 represents the outer beam radius at the anode and is estimated from the unperturbed distribution of (12), and γ_0 is the related beam angle. In the present work, (13) was used to estimate the beam broadening. In all cases considered in this paper, the beam broadening $\Delta\rho$ at the outer radius (i.e., $\rho = \rho_0$) was less than 10% of the beam outer radius ρ_0 . Thus, the exclusion of space-charge spreading in the present study is reasonable.

An energy moment of (12) provides the rate of energy deposition in the anode per unit area

$$q''(\rho) = A_c \int_{E_{min}}^{\infty} (E - \mu_a) G(\rho, E) dE. \quad (14)$$

The foregoing relation could be used to provide a Neumann boundary condition for the description of heat transfer in the anode. However, in many cases of interest, the electron energies are sufficiently high to enable ballistic or quasiballistic transport into the depth of the anode. Consequently, we treat the deposition of energy as a volumetric phenomenon using the Monte Carlo method described below. The integral in (14) can be simplified to a good approximation by recognizing the narrowness of the energy distribution $F(\theta, E)$, which varies by only a few tenths of eV about the chemical potential of the cathode μ_c [19]. Thus, for $V \gg 0.1$ V, the energy difference $(E - \mu_a)$ can be replaced by qV to a good approximation. Importantly, this approximation satisfies conservation of total energy input $Q = IV$, but the approach ignores heating or cooling of the cathode via the Nottingham effect [20].

B. Electron Scattering

Energetic electrons impact the anode surface and lose energy through a series of scattering events within the surface of the anode. Each inelastic collision involves an exchange of energy with the lattice, resulting in localized heating of the anode. The electron path and energy exchange are used to predict the heating rate as a result of electron bombardment.

Detailed electron scattering models have been developed for applications in scanning electron microscopy. These studies generally involve electrons of higher energy than those considered here. Nevertheless, the general methods employed, such as the Monte Carlo method described below, are applicable to the present work. The subject of electron scattering has been studied extensively [21]–[23], and in the following paragraphs, we summarize concisely the approach taken in the present work.

A Monte Carlo approach describing the path and energy loss of the electrons is used in the present work. Tabulated values of Mott cross-sections for elastic scattering [24] in the anode

material (assumed to be aluminum) provide a means of computing scattering probabilities, elastic mean free paths for electron flight and scattering angles. Because the anode is a metal, the interior potential gradient is negligible, and the trajectory follows a straight line between collisions. During the free-flight of the electron, inelastic scattering is included using a modified Bethe continuous energy loss relation [25], [26].

The determination of electron energy E at anode impact was described previously. Because of the narrow energy range of emitted electrons, the energy of impacting electrons is assumed to be $qV + \mu_c$. With this initial energy, the Monte Carlo simulation of collisions proceeds until the electron energy reaches the anode's chemical potential μ_a . Each electron's initial position is determined from the spatial distribution given by (11). The direction of the electrons is assumed to be normal to the anode surface. This assumption is reasonable because the emitted distribution from the cathode is highly oriented in the surface-normal direction ($\theta = 0$) and because the electric field accelerates the electrons in this same direction.

Individual electrons are tracked independently in the present formulation, and, consequently, electron-electron scattering is ignored. For each collision with the lattice, the location is recorded, and amount of the energy lost by the electron is added to the lattice. The energy transferred from the electron to the lattice appears in the heat diffusion equation as a generation term (see below). The spatial distribution of energy deposition is then added to prior trajectories. To achieve convergent results with smooth contours of energy deposition, many electrons trajectories (typically 10^6) were simulated. The resulting distribution of energy deposition was then normalized to reflect an average energy per volume per electron in the generation region. This normalized volumetric energy was then multiplied by the total current I to obtain a volumetric heat generation distribution.

C. Thermal Diffusion

The heat transfer is governed by the diffusion equation using the electron scattering results as a generation term G . The field emission process is assumed to be at steady state, so transient effects in the generation are ignored. However, transient thermal effects are captured with the foregoing model

$$\rho C_p \frac{\partial T}{\partial t} = \nabla \cdot (k \nabla T) + G \quad (15)$$

where C_p and k are the bulk specific heat and thermal conductivity of the anode (aluminum).

An array of tip emitters will produce an inherently three dimensional heating pattern and subsequent temperature profile in the anode. The case considered here, however, is only concerned with the heating caused by a single tip emitter. Therefore the conduction solution is assumed to be axisymmetric whose axis of symmetry coincides with that of the electron beam. Because the heating that occurs is highly localized, the conduction domain is assumed to be semi-infinite. This is only possible if a single emitter is considered because conduction from neighboring emitters would pollute the reduced-dimension solution.

The single emitter assumption further simplifies the problem because the analytic solution to a point source can be recovered

far from the generation region. As a result, the boundary conditions far from the generation region can be assumed to be the Green's function solution to a point source at the location of impingement given as

$$T(r) = \frac{Q}{2\pi kr} \quad (16)$$

where k is the thermal conductivity of aluminum and Q is the total heat input (in W). In this case, the voltage across the gap times the emitted current yields a Joule heating term ($Q = IV$) that is treated as a point source. Even though this solution is one-dimensional (1-D) because the temperature only depends on the distance from the generation point source, the temperature field near the generation region will still be two-dimensional (2-D). At the far field boundaries of the 2-D conduction region, the solution is assumed to depend on radial distance from the origin only. Therefore, the domain must be large enough to approximate 1-D conduction at the edges.

Because the generation predicted by the Monte Carlo simulation is an arbitrary function of depth into the anode and radial distance from the beam centerline, the solution for the conduction was calculated numerically using a general finite element PDE solver library in C++ [27]. The meshing for the numerical solution was crucial to be able to resolve the small scale region of generation predicted by the Monte Carlo solution. At the centroid of each element in the generation region, an interpolated value was selected from the bins of the Monte Carlo simulation. To ensure that energy was conserved, the total energy generated in all elements was scaled to equal the Joule heating term (g) calculated previously, which approximately represents the energy deposited into the anode.

III. RESULTS AND DISCUSSIONS

Simulation of anode heating requires knowledge of the distribution of electron deposition described by (12). Fig. 2 contains a graph of the current density (with a logarithmic scale) as a function of radial position on the anode. The curves in the figure correspond to several values of the cathode-anode spacing L at a voltage bias of 50 V with a field enhancement factor $\beta = 750$. The strong influence of this spacing on current density is clearly evident, as the smallest spacing ($L = 5 \mu\text{m}$) produces local current densities that are more than ten orders of magnitude greater than those predicted for the largest spacing ($L = 20 \mu\text{m}$). This phenomenon is a consequence of the exponential dependence of field-emission current on electric field. Under the conditions of constant voltage bias, the field is inversely proportional to the spacing L . We also observe a relatively narrow spatial distribution of current density. The figure illustrates that the effective radius of electron impact ranges from 1 to $2.5 \mu\text{m}$, depending on the cathode-anode spacing.

In the case of variable spacing L under a constant electric field V/L , the emitted current remains constant while the voltage bias V and the resulting electron energy E scale with the spacing. Fig. 3 contains a graph of the current density as a function radial position on the anode under the condition of constant electric field at several values of L . The figure illustrates the broadening of the constant total current with distance L . For the smallest

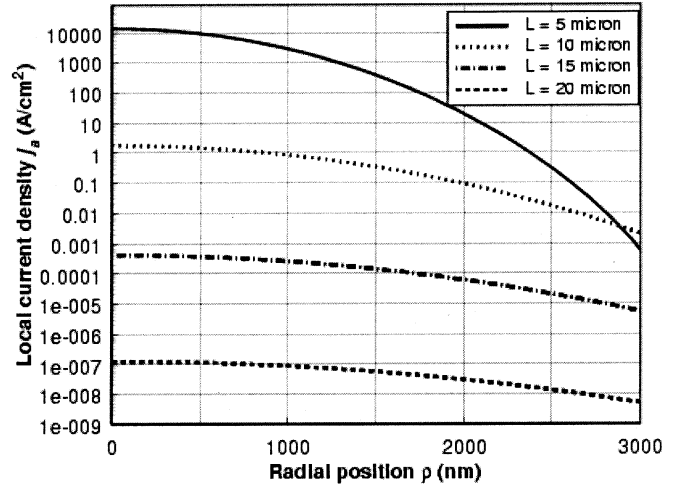


Fig. 2. Current density j_a as a function of radial position ρ and cathode-anode separation L . Constant voltage bias $V = 50$ V for all cases.

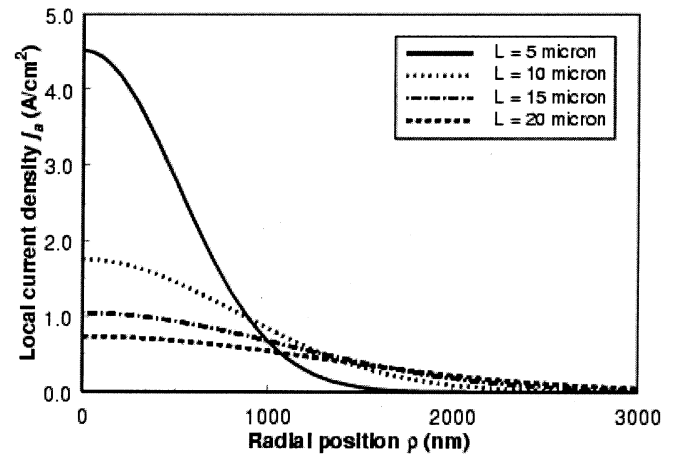


Fig. 3. Current density j_a as a function of radial position ρ and cathode-anode separation L . Constant applied field $V/L = 5$ V/ μm for all cases.

spacing, most of the current exists within $\rho < 1 \mu\text{m}$. As the spacing increases, the current spreads to approximately $3 \mu\text{m}$. Also, the peak current density, which can strongly influence localization of heat dissipation, decreases from 4.5 A/cm^2 for $L = 5 \mu\text{m}$ to less than 1 A/cm^2 for $L = 20 \mu\text{m}$. Further, in this case of constant electric field, the dissipated energy per electron, $(E - E_{fa}) \approx qV$, increases with the spacing L , and the resulting total heat dissipation scales with V .

For the Monte Carlo simulation, electrons were chosen at random from the distributions in Figs. 2 and 3 where the initial energy is the voltage across the gap plus the fermi-level of the cathode (assumed to be 5 eV). The distribution of energy deposited into the anode through scattering can be seen in Fig. 4 for an applied field of $5 \text{ V}/\mu\text{m}$. In the distribution shown, 10 million electrons were used to achieve the smooth contours.

The size of the 2-D (axisymmetric) conduction domain was 2000 nm in radius and 2000 nm in depth. The size was determined by evaluating the calculated maximum temperature for various dimensions. As the radius and/or depth increase, the boundaries approach the 1-D solution and the maximum temperature is said to be converged. The meshing was determined

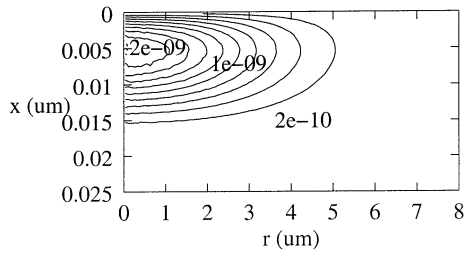


Fig. 4. Normalized energy distribution in ($\text{eV}/\text{e}^-/\text{nm}^3$) from electron scattering in aluminum for an initial energy of 100 eV. The electron beam is centered at the origin (top left side of the plot).

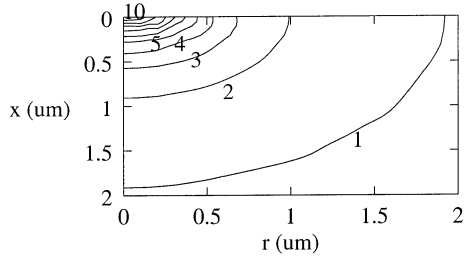


Fig. 5. Temperature distribution using generation from Fig. 4 ($10 \text{ V}/\mu\text{m}$ case) and boundary conditions from the 1-D analytic conduction solution to a point source.

TABLE I
ELECTRICAL CURRENT, MAXIMUM TEMPERATURE RISE AND HEAT FLUX FOR GIVEN APPLIED VOLTAGE AND ELECTRODE SPACING

Voltage (V)	Gap (μm)	Current (A)	ΔT_{max} (K)
25	5	7.48×10^{-8}	0.01
50	5	2.78×10^{-4}	28.08
100	20	7.48×10^{-8}	0.01

by the requirement of a converged conduction solution as well as accurate representation of the generation region. A coarse mesh of 45 nodes in each direction was augmented by a refinement in the generation region. The final element size in the generation region did not exceed 0.3 nm in the z -direction with 9179 total elements. Despite the lack of resolution, the peak temperature was found to be constant at steady state for several differing mesh sizes. As described in the Theory section, energy was conserved by scaling the values in the finite elements so that the integral of the energy was equal to the Joule term. For the $10 \text{ V}/\mu\text{m}$ case, the energy generation was 0.0124 W.

The finite element temperature solution appears in Fig. 5. Note the spherical temperature solution away from the heat source. The maximum temperature rise occurs in the generation region and is calculated to be $\Delta T_{\text{max}} = 28.08 \text{ K}$. Although this value by itself is not indicative of possible failure, the heating is highly localized. The maximum heat flux in the system is approximated to be $q_{\text{max}} = 470 \text{ kW}/\text{cm}^2$.

Table I shows the temperature rise for various voltage and electrode spacing configurations. In addition, the heat flux and current are reported. For all test cases except the $10 \text{ V}/\mu\text{m}$ case, the heating was insignificant (see Table I). This is a result of the fact that the current is a strong function of the applied field, so the energy deposited, which is proportional to the current, is also a strong function of the applied field.

IV. CONCLUSION

A description of the mechanism of anode heating in field emission devices has been demonstrated using electron field emission theory, Monte Carlo simulation of electron scattering, and thermal diffusion. The present analysis determines the electron number distribution and energy based on emission from geometrically enhanced tips. The bombardment and subsequent heating of the anode is considered by thermalizing energetic electrons in a stochastic scattering process. Temperature distributions in the anode are then obtained through a numerical conduction solution using the deposited electron energy as a source.

The predicted temperature increases from a single emitter do not indicate failure by melting. However, the large local heat fluxes and temperature gradients in the anode suggest that thermal stresses may become significant. This subject could form the basis of a future study. The present work provides a foundational formulation and several examples of practical devices. The possible range of voltages and electrode spacings in practical devices is very large. Further, the presence of multiple emitters in an array is also common in practical devices. Thus, further studies could consider these effects explicitly. The present work has demonstrated a strong effect of voltage on heating due to the exponential current-voltage relationship in field emission devices. Thus, we anticipate that practical devices, particularly those operating at high current density, could encounter substantial thermal damage.

REFERENCES

- [1] I. Brodie and P. R. Schwoebel, "Vacuum microelectronic devices," *Proc. IEEE*, vol. 82, pp. 1006–1018, 1994.
- [2] J. A. Nation, L. Schachter, F. M. Mako, L. K. Len, W. Peter, C.-M. Tang, and T. Srinivasan-Rao, "Advances in cold cathode physics and technology," *Proc. IEEE*, vol. 87, pp. 865–889, 1999.
- [3] R. H. Fowler and L. W. Nordheim, "Field emission from metallic surfaces," in *Proc. Royal Soc. A*, vol. 119, 1928, pp. 173–181.
- [4] C. A. Spindt, "A thin film field emission cathode," *J. Appl. Phys.*, vol. 39, pp. 3504–3505, 1968.
- [5] K. L. Jensen, "Field emitter arrays for plasma and microwave source applications," *Phys. Plasmas*, vol. 6, no. 5, pp. 2241–2253, 1999.
- [6] K. L. Jensen, J. E. Yater, E. G. Zaidman, M. A. Kodis, and A. Shih, "Advanced emitters for next generation rf amplifiers," *J. Vac. Sci. Technol. B*, vol. 16, no. 4, pp. 2038–2048, 1998.
- [7] Q. H. Wang, A. A. Setlur, J. M. Lauerhaas, J. Y. Dai, E. W. Seelig, and R. P. H. Chang, "A nanotube-based field emission flat panel display," *Appl. Phys. Lett.*, vol. 72, no. 22, pp. 2912–2913, 1998.
- [8] S. Z. Deng, Z. S. Wu, N. S. Xu, and J. Chen, "Characterization of a high voltage flat panel display unit using nanotube-based emitters," *Ultramicroscopy*, vol. 89, no. 1–3, pp. 105–109, 2001.
- [9] W. P. Kang, T. S. Fisher, and J. L. Davidson, "Diamond microemitters—the new frontier of electron field emissions and beyond," *New Diamond Frontier Carbon Technol.*, vol. 11, no. 2, pp. 129–146, 2001.
- [10] A. Wisitsora-at, W. P. Kang, J. L. Davidson, D. V. Kerns, and T. S. Fisher, "Diamond field emission triode with low gate turn-on voltage and high gain," *J. Vac. Sci. Technol. B*, to be published.
- [11] S. B. Sinnott and R. Andrews, "Carbon nanotubes: synthesis, properties, and applications," *Critical Rev. Solid State Mater. Sci.*, vol. 26, no. 3, pp. 145–249, 2001.
- [12] M. S. Dresselhaus, "Burn and interrogate," *Science*, vol. 292, no. 5517, pp. 650–651, Apr. 2001.
- [13] W. Zhu, C. Bower, O. Zhou, G. P. Kochanski, and S. Jin, "Large current density from carbon nanotube field emitters," *Appl. Phys. Lett.*, vol. 75, no. 6, pp. 873–875, 1999.
- [14] J. M. Bonard, H. Kind, T. Stockli, and L. A. Nilsson, "Field emission from carbon nanotubes: the first five years," *Solid-State Electron.*, vol. 45, no. 6, pp. 893–914, 2001.

- [15] W. Zhu, C. Bower, G. P. Kochanski, and S. Jin, "Field emission properties of diamond and carbon nanotubes," *Diamond Related Mater.*, vol. 10, pp. 1709–1713, 2001.
- [16] P. Grant, C. Py, C. Mößner, A. Blias, H. Tran, and M. Gao, "Electron field emission from diamond-like carbon, a correlation with surface modifications," *J. Appl. Phys.*, vol. 87, no. 3, pp. 1356–1360, Feb. 2000.
- [17] R. H. Good and E. W. Müller, "Field emission," in *Encyclopedia of Physics*, S. Flugge, Ed. Berlin, Germany: Springer-Verlag, 1956, vol. 21, pp. 176–231.
- [18] G. H. Jansen, "Coulomb interactions in particle beams," *Nucl. Instrum. Methods Phys. Res. A—Accelerators Spectrometers Detectors Assoc. Equip.*, vol. 298, no. 1–3, pp. 496–504, Dec. 1990.
- [19] J. W. Gadzuk and E. W. Plummer, "Field-emission energy-distribution (feed)," *Rev. Modern Phys.*, vol. 45, pp. 487–548, 1973.
- [20] W. B. Nottingham, "Remarks on energy loss attending thermionic emission of electrons from metals," *Phys. Rev.*, vol. 59, pp. 906–907, 1941.
- [21] J. W. Motz, H. Haakon Olsen, and H. W. Koch, "Electron scattering without atomic or nuclear excitation," *Rev. Modern Phys.*, vol. 36, no. 4, pp. 881–927, Oct. 1964.
- [22] A. J. Antolak and W. Williamson Jr., "Electron backscattering from bulk materials," *J. Appl. Phys.*, vol. 58, no. 1, pp. 526–534, July 1985.
- [23] J. C. Kuhr and H. J. Fitting, "Monte Carlo simulation of low-energy electron scattering in solids," *Phys. Status Solidi A—Appl. Res.*, vol. 172, no. 2, pp. 433–449, 1999.
- [24] Z. Czyzewski, D. O. MacCallum, A. Romig, and D. C. Joy, "Calculations of Mott-scattering cross-section," *J. Appl. Phys.*, vol. 68, no. 7, pp. 3066–3072, 1990.
- [25] D. C. Joy and S. Luo, "An empirical stopping power relationship for low-energy electrons," *Scanning*, vol. 11, no. 4, pp. 176–180, July 1989.
- [26] H. A. Bethe, "Theory of passage of particles through matter," *Annu. Phys.*, vol. 5, pp. 325–400, 1930.
- [27] H. P. Hans Petter Langtangen, *Computational Partial Differential Equations: Numerical Methods and Diffpack Programming*. Berlin, Germany: Springer, 1999.

Timothy S. Fisher received the M.S. degree from Vanderbilt University, Nashville, TN, in 2002 and the Ph.D. degree from Cornell University, Ithaca, NY, in 1998.

He joined the Purdue faculty as an Associate Professor and member of the Birck Nanotechnology Center in 2002 after several years at Vanderbilt University, Nashville, TN (1998–2002). Prior to his graduate studies, he was employed from 1991 to 1993 as a Design Engineer in Motorola's Automotive and Industrial Electronics Group. His current research includes work on simulation and measurement of nanoscale heat transfer, coupled electro-thermal effects in semiconductor devices, nanoscale direct energy conversion, molecular electronics, microfluidic devices, and boundary- and finite-element computational methods. His research efforts include theoretical, computational, and experimental approaches and have been sponsored by National Science Foundation, the Defense Advanced Research Projects Agency, the Army Research Office, the National Reconnaissance Office, the US Air Force, the Tennessee Valley Authority, 3M, and the Semiconductor Research Corporation. He holds three U.S. patents.

Dr. Fisher received the CAREER Award from the National Science Foundation and a Nontenured Faculty Award from 3M, a Graduate Fellowship, and Best Student Poster Award from the Semiconductor Research Corporation. He is a member of Tau Beta Pi and Pi Tau Sigma. He serves on the IEEE TC-9 Committee on Thermal Phenomena in Electronics, the ASME K-6 Committee on Heat Transfer in Energy Systems, and the ASME K-16 Committee on Thermal Management of Electronics.

D. G. Walker is an Assistant Professor of mechanical engineering at Vanderbilt University, Nashville, TN, with interests in energy transport at small scales, simulation of microelectronic device physics, and direct energy conversion technologies.

Robert A. Weller is an Associate Professor of electrical engineering at Vanderbilt University, Nashville, TN, with interests in radiation effects in solids, ion beam fabrication and analysis of materials, electronic materials, and computer simulation of radiation effects in materials and devices.